Lawrence Berkeley National Laboratory

Lawrence Berkeley National Laboratory

Title

SQUID-Detected MRI at 132 Microtesla with T1 Contrast Weighted at 10 Microtelsa-300 mT

Permalink

https://escholarship.org/uc/item/3hn90152

Authors

Lee, SeungKyun
Moessle, Michael
Myers, Whittier
et al.

Publication Date

2004-08-09

Peer reviewed

eScholarship.org Powered by the California Digital Library
University of California

SQUID-Detected MRI at 132 μT with T_1 contrast weighted at 10 μT-300 mT

SeungKyun Lee[1,2], Michael Möβle[1,2], Whittier Myers[1,2], Nathan Kelso[1,2], Andreas H. Trabesinger[3], Alexander Pines [4], and John Clarke[1,2]

Departments of [1]Physics and [4]Chemistry, University of California, Berkeley, CA 94720, USA
[2]Materials Sciences Division, Lawrence Berkeley National Laboratory, Berkeley, CA 94720, USA
[3]ETH Zurich, Laboratory of Physical Chemistry, CH-8093 Zurich, Switzerland

[Running head]
SQUID-Detected T_1-Contrast MRI

[Corresponding author]
SeungKyun Lee
366 LeConte Hall, UC Berkeley,
Berkeley, CA 94720
510 – 642 – 3634 (phone)
510 – 642 – 1304 (fax)
lsk@socrates.berkeley.edu

Abstract

T_1-weighted contrast MRI with prepolarization was detected with a superconducting quantum interference device (SQUID). A spin evolution period in a variable field between prepolarization and detection enabled the measurement of T_1 in fields between 1.7 μT and 300 mT; T_1 dispersion curves of agarose gel samples over five decades in frequency were obtained. SQUID detection at 5.6 kHz drastically reduces the field homogeneity requirements compared to conventional field-cycling methods using Faraday coil detection. This allows T_1 dispersion measurements to be easily combined with MRI, so that T_1 in a wide range of fields can be used for tissue contrast. Images of gel phantoms with T_1-weighted contrast at four different fields between 10 μT and 300 mT demonstrated dramatic contrast enhancement in low fields. A modified inversion recovery technique further enhanced the contrast by selectively suppressing the signal contribution for a specific value of the low-field T_1.

Key words: low-field MRI, SQUID, T_1-weighted contrast, relaxation dispersion

The nuclear spin-lattice relaxation time T_1 is determined by the spectral density of local magnetic field fluctuations at the NMR frequency (1). Random fluctuations caused by molecular motion and chemical exchange occurring on the time scale of the correlation time τ_c have strong spectral components up to $\omega \approx 1/\tau_c$. While in pure water $\tau_c \sim 1$ ps, in many tissues and macromolecular solutions τ_c ranges from a fraction of a microsecond to a millisecond. Hence, at frequencies of 1 MHz or lower T_1 is sensitive to the molecular environment and interactions specific to tissue types. On the other hand, at frequencies of about 10 MHz or higher, the relaxation times of different tissues tend to converge because of the decoupling of the proton spins from most of the important relaxation mechanisms available in biological samples.

The enhancement of T_1 contrast at low frequencies is an important reason for continued interest in low-field MRI (2-4), together with the low-cost implementation of MRI without the need for a superconducting magnet. Moreover, the study of the relaxation rates over a broad range of frequencies, known as relaxation dispersion, has proven to be a valuable tool to provide insight into the dynamics and structure of tissues and protein solutions (5-7). Because of the severe loss in sensitivity of a Faraday coil at low frequencies and the low level of magnetization available in low fields, conventional fixed-field MRI performs poorly in fields less than about 0.1 T and does not lend itself well to the investigation of relaxation times and T_1-weighted contrast imaging at significantly lower fields.

The loss of sensitivity in low-field NMR and MRI can be partially alleviated by using a separate pulsed polarization field, which provides a sample magnetization that is independent of the detection field B_0 (2,3,8). The Ljubljana group (8) used this technique to perform MRI in the Earth's magnetic field, and was able to show enhanced T_1-weighted contrast in a gelatin sample. However, the poor signal-to-noise ratio (SNR) obtained by Faraday coil detection in the Earth's field, even with prepolarization, severely limited the resolution and practical applicability of the method.

Low- to intermediate-field T_1-dispersion has been extensively studied by means of field cycling methods (5-7) in which a low-field spin evolution period precedes a high-field detection period. This requires a highly homogeneous, strong, pulsed field in which to detect the NMR,

requirements that are often incompatible with high speed imaging of large samples. To study localized T_1 dispersion *in vivo* in the relatively narrow range from about 20 to 120 mT, Carlson *et al*. (9) pulsed an inhomogeneous field (30% variation over the imaging volume) inside the bore of a commercial fixed-field (64 mT) MRI magnet. They observed pronounced peaks in the relaxation dispersion behavior of rat and human tissues, which they ascribed to cross-relaxation of ^{1}H with ^{14}N. To probe T_1 dispersion in a field much lower than the detection field, however, a pulsed field with much higher homogeneity would be necessary for reasonably uniform cancellation of the static field.

In an alternative approach, Rommel *et al*. (10) investigated contrast that is sensitive to the low-frequency (<10 kHz) dynamics of tissue molecules using the spin-lattice relaxation time in the rotating frame ($T_{1\rho}$). The low-frequency dispersion of $T_{1\rho}$ has the advantage of being accessible in conventional MRI using RF irradiation, but the frequency range is limited by the available RF power and by tissue heating. Furthermore, the interpretation of $T_{1\rho}$-weighted images is less straightforward than that of T_1-weighted images.

To detect MRI at low fields, a complementary approach to sample prepolarization is to address the poor performance of conventional Faraday coil detection at low frequencies. Recently, we have demonstrated MRI in a microtesla detection field (11,12) by combining prepolarization of the spins and signal detection with an untuned SQUID magnetometer. A similar approach was taken by the Los Alamos group (13) to obtain NMR signals from a human brain at a few hundred Hz. As SQUID detection is independent of frequency and prepolarization provides magnetization independent of the detection field, this technique allows the detection field B_0 to be as low as ~100 μT, limited primarily by the requirement that $f_0 >> \Delta f$, where f_0 is the Larmor frequency and Δf is the imaging bandwidth. Since the homogeneity requirement for the pulsed polarization field is modest and B_0 is very weak, inexpensive copper-wire coils can provide adequate fields for open-access MRI of objects the size of human limbs. In our earlier work we obtained two-dimensional images of phantoms and vegetables (with sample size ~ 50 mm, B_0 = 132 μT, f_0 = 5.6 kHz, and maximum gradient G = 75 μT/m) with millimeter resolution in a few minutes.

In this communication we demonstrate a new scheme for T_1-weighted contrast MRI that enables one to use T_1 over a wide range of fields for image contrast. By applying an intermediate field between prepolarization and detection we obtain images weighted by T_1 in an arbitrary field strength ranging from the 300 mT-prepolarization field to about 10 μT. We illustrate this principle by measuring T_1 dispersion and acquiring T_1-weighted contrast images of agarose gels with varying water content. Finally, we make use of a modified inversion-recovery sequence based on that proposed by Planinšič *et al.*(8), which we call a "field-cycling inversion recovery" sequence, to obtain high-contrast images with selective suppression of different portions of the phantom according to their relaxation rate in a field of 132 μT.

EXPERIMENT

SQUID-Detected Microtesla-Field MRI: System Configuration

We briefly describe the essential features of microtesla-field MRI using a SQUID; details have been published elsewhere (11,12). Figure 1a shows a schematic of the SQUID probe and detection electronics. The multiturn Nb input coil (ic) of a low transition-temperature (T_c) SQUID (sq) with Nb-AlOx-Nb trilayer junctions is connected to a superconducting flux transformer (pickup coil, pc) wound from Nb wire. The transformer is configured as a second-order axial gradiometer – consisting of 1 + 2 + 1 turn coils with 65-mm diameter and 150 mm separation between the two single-turn coils – to attenuate magnetic field noise from distant sources without materially reducing the signal field from the nearby sample. The magnetic field from the precessing spins in the sample causes a supercurrent to flow in the lowest coil, and hence in the input coil. A series array of twenty Josephson junctions is inserted between the pickup coil and the input coil to limit the supercurrent in the input coil generated by pulsed fields. Both the SQUID and the array are placed in a superconducting shield to prevent their direct exposure to external fields. The SQUID probe is immersed in liquid helium in a custom-made low-noise cryostat (14) with 25 mm separation between the lower loop of the gradiometer and the room temperature surface of the cryostat. The voltage signal from the current-biased SQUID is read out by room-temperature electronics using a conventional flux-locked loop with

flux modulation at 2 MHz (15). The measured magnetic field noise of the system, 1.7 fT/Hz$^{1/2}$ referenced to the lowest pickup loop, arises from the noise of the SQUID itself.

The cryostat is placed at the center of the 2 m cubical wooden structure shown in Fig. 1b. The cube supports the coils necessary for MRI in an open space: three pairs of coils to null out the Earth's field (wound on the faces of the cube), a Helmholtz pair with a 0.6 m radius for B_0, three sets of gradient field coils, a prepolarization field coil, and a coil to produce pulses of the excitation field $2B_1\cos\omega_0 t$. An aluminum box with 3-mm thick walls surrounds the cube to attenuate spurious 5.6 kHz electromagnetic fields by an order of magnitude.

Pulse Sequences

Figure 2a shows the simplest pulse sequence for MRI in microtesla fields with contrast weighted by T_1 in a variable field between ~1 μT and ~300 mT. The spins are first fully polarized in a relatively strong field B_{p1} ~300 mT applied for a time t_p greater than the longest T_1 in the sample; B_{p1} is generated by applying 40 A to a copper solenoid of inner diameter 50 mm which surrounds the sample. For T_1 contrast in a field greater than B_0 = 132 μT, the polarizing field is reduced adiabatically to B_{p2} to create an intermediate field $\mathbf{B_{int} = B_{p2} + B_0}$ under which the spins relax for time t_{int}. Since the polarizing field is perpendicular to $\mathbf{B_0}$, $\mathbf{B_{int}}$ is at an angle $\theta = \tan^{-1}(B_{p2}/B_0)$ to $\mathbf{B_0}$. The adiabatic switching of the fields ensures that the spin magnetization is always in the direction of the instantaneous field. The magnetization preparation is completed by adiabatically switching off B_{p2}, thereby causing the spins to align along the direction of B_0. The magnetization at this point

$$M_1 = M_{\text{int}} + (M_{p1} - M_{\text{int}}) \exp(-t_{\text{int}} / T_{1,\text{int}}) \qquad [1]$$

determines the intensity of the image, which is subsequently obtained by applying a conventional spin-echo spin-warp imaging sequence. In Eq. [1], M_{int} and M_{p1} are the equilibrium magnetizations in B_{int} and B_{p1}, respectively, and $T_{1,\text{int}}$ is the spin-lattice relaxation time in B_{int}. Note that if $B_{\text{int}} = B_0$, the pulse sequence probes the T_1 contrast in the field B_0 during the time t_{int}, which is equivalent to the delay time t_d in the images in ref. (11,12). To achieve contrast

weighted by T_1 in fields lower than B_0, the corresponding intermediate field $B_{int} < B_0$ is obtained by setting $B_{p2} = 0$ and temporarily reducing B_0 by applying a counter-field by means of one of the Earth's field cancellation coils for time $t_{int.}$ After this period, the field is ramped back to the original B_0, and the imaging sequence follows.

The above scheme produces little contrast if (M_{p1}-M_{int}) is small. To achieve T_1-weighted contrast in a field comparable to the maximum B_{p1} ~300 mT, one can simply use that field for prepolarization, and adjust the polarization time such that spins with differing T_1 in that field have different polarizations when B_{p1} is turned off. This is equivalent to changing the repetition time in conventional MRI.

Conventional high-field MRI frequently utilizes inversion recovery to highlight T_1-weighted contrast. A related technique, originally called "magnetization subtraction" by Planinšič *et al*.(8), can be used to enhance the low field contrast in prepolarization MRI if pulsed fields are available. Figure 2b illustrates the magnetization preparation in this sequence, which we dub a "field-cycling inversion recovery" sequence. As before, the spins are first polarized in a strong field B_{p1}. This field is adiabatically removed to allow the spins to align along the static field B_0. For a time t_{int}, the spins relax in B_0 until a resonant π pulse creates population inversion. Immediately following the inversion, a second polarization field B_{p2} is adiabatically switched on, whereupon the inverted magnetization recovers towards thermal equilibrium in B_{p2}. The zero-crossing point is determined by both the magnetization immediately before the π pulse and the relaxation time in B_{p2}. Finally, the field is adiabatically switched back to B_0, and the standard imaging sequence is implemented.

The usefulness of this technique lies in the fact that even if different parts of the sample (tissues) have very similar relaxation times in high fields of B_{p1} and B_{p2}, the zero crossing points can be significantly different depending on their magnetization immediately before the π pulse, which is determined by the relaxation time in B_0. Hence by choosing an appropriate second polarization time t_{p2}, tissue-selective suppression of the image intensity is possible by exploiting the differences in low-field T_1. Note that the low-field evolution during t_{int} can be made to occur in a

field other than B_0, as in Fig. 2a, by adding a nonzero field from the polarization coil or by reducing the current to the B_0 coil.

MATERIALS

In our initial experiments, phantoms composed of agarose gel (Sigma-Aldrich, A9539-25G) were used to demonstrate the principle of the sequences explained above. Because of the slow motion of cross-linked polymer chains, the gel has a correlation time similar to those found in tissues, and one can easily produce different relaxation times by changing the concentration of the gel. In a simplified picture, the relaxation rate can be expressed as (16)

$$1/T_1 = (1-b)/T_{1f} + b/T_{1b}, \qquad [2]$$

where T_{1f} and T_{1b} are the relaxation times of free water and water bound to the gel, respectively, and b is the fraction of the bound water (typically < 1%). For NMR frequencies above ~10 kHz $1/T_{1f}$ is independent of frequency. However, $1/T_{1b}$ sharply increases below a frequency of about $1/\tau_c$, which is of the order of 1 MHz. Therefore, low-field relaxation is sensitive to the bound water fraction b, which in turn is determined by the gel concentration.

RESULTS

Figure 3a shows $1/T_1$ dispersion curves of agarose gel samples (0.5% and 0.25% by weight in H_2O) over the frequency range 72 Hz to 12.8 MHz. To measure T_1 at a given field, we used the pulse sequence of Fig. 2a without image encoding and measured the signal amplitude for increasing values of t_{int}. An exponential fit of that dependence determined T_1 at the selected magnetic field B_{int}. The solid lines are fitted to the data using the Cole-Cole expression (5)

$$1/T_1(f) = A \cdot \mathrm{Re}\{1/[1+(if/f_c)^{\beta/2}]\} + \text{constant}, \qquad [3]$$

where A, f_c, β, and the constant are fitting parameters. This relation successfully describes the relaxation dispersion of many tissues and diamagnetic protein solutions in which a distribution of correlation times is often required to characterize the fluctuations. The fits give characteristic time scales (obtained from the inflection points of the fitted curves) for molecular motion of 3 μs and 2 μs for the 0.25% and 0.5% gels, respectively. At high frequencies the relaxation rates have a frequency-independent component arising from the relaxation of free water (the first term in Eq. [2]). Below a frequency ~0.1 MHz the second term in Eq. [2] dominates the relaxation rate and the curves show sharp rises with strong dispersion, with the relaxation rate roughly proportional to the gel concentration.

We turn now to illustrations of T_1-weighted contrast imaging. Figure 3b shows images of two glass tubes filled with 0.25% and 0.5% gels, respectively, weighted by T_1 at four different fields in the range 10 μT to 300 mT. The images were obtained using the sequence of Fig. 2a with the different intermediate field strengths indicated in the figure. Thirty-one phase encoding steps were used with no signal averaging; the total data acquisition time was 1.5 minutes for each image. As is expected from the relaxation dispersion curves of Fig. 3a, the contrast is much stronger in the images with the lower fields of 10 μT and 132 μT. The two plots at the bottom of the figure show the image intensities along the lines across the two bottom images. The contrast (defined as the difference in peak heights divided by the larger of the two) between different gel components yields 36% for the image with B_{int} = 132 μT and 7% for that with B_{int} = 13.2 mT.

To obtain Fig. 4, we filled three glass tubes with tap water, 0.25% agarose gel, and 0.5% agarose gel, respectively, and imaged them with the conventional spin-echo spin-warp sequence preceded by the field-cycling inversion recovery sequence of Fig. 2b. Whereas all three samples have approximately the same relaxation time, $T_1 = 1.8 \pm 0.1$ sec, in the polarizing field $B_{p1} = B_{p2}$ = 300 mT, T_1 varies greatly in B_0 = 132 μT (1.6 sec, 480 ms, and 210 ms for water, 0.25% gel, and 0.5% gel, respectively). In each image, the length of the second polarizing pulse, t_{p2}, has been chosen so that the polarization of one of the samples vanishes at the end of the inversion-recovery sequence. As t_{p2} is increased, each of the three samples appears dark in turn, from shorter to longer T_1, as a result of the successive zero-crossings of the magnetization. In

addition, in all three images there is sufficient T_1 contrast to discriminate between the two non-vanishing columns.

DISCUSSION

We have demonstrated that by detecting spin precession in an ultra-low field with a SQUID and employing pulsed polarization fields to manipulate the longitudinal magnetization, one can obtain T_1-weighted contrast images in fields between 10 μT and 300 mT, corresponding to proton Larmor frequencies of 426 Hz and 12.8 MHz. Since the image encoding and detection are performed in a very low static field, the homogeneity requirement on the pulsed fields is modest. This key fact allows one to use T_1 dispersion in a wide range of fields as a source of image contrast in larger samples than can be used in conventional field-cycling relaxometers. The lower limit on the field is set by the low-frequency environmental field fluctuations that significantly contribute to the spin relaxation when the Larmor frequency is below about 100 Hz. The heat generated by the polarization coil sets the upper limit on the field. With moderate magnetic shielding and a water- or nitrogen- cooled polarization coil, the field range in which T_1 -weighted contrast images are obtained could be further expanded.

Currently we can image samples up to 50 mm in diameter with in-plane resolution of 1-4 mm in about 2 minutes. Considerable SNR improvement would be necessary to improve the resolution or decrease the acquisition time for clinically relevant *in vivo* imaging. Reducing the system noise by using a lower-noise SQUID and increasing the filling factor by using a dewar with a smaller vacuum gap would improve the SNR by a factor of 2-4. More efficient cooling of the polarization coil could increase the available field for prepolarization to up to ~0.5 T (2). These improvements could potentially be combined with a multichannel system in which many SQUID gradiometers would be used to cover a larger field-of-view. Such a system could potentially complement conventional high-field MRI in areas such as *in vivo* relaxometry and tumor screening.

SQUID-detected low-field MRI with the flexibility of widely variable polarization fields is well suited for exploring other contrast modalities that are not exploited in conventional MRI

experiments. In addition to the generally enhanced contrast in low fields, extensive studies have shown rich structure in the T_1 dispersion curves of both living and excised tissues (17), suggesting possibilities of novel contrast mechanisms provided one can fine tune the field – particularly at low fields. For example, dips in the proton T_1 dispersion curves at ^{14}N quadrupolar transition frequencies caused by cross relaxation with nitrogen (18) can be used to identify nitrogen-containing protein backbones. Furthermore, T_1 dispersion contrast, which measures the slope of the T_1 dispersion curve, can be used to produce tissue-specific contrast when samples exhibit complex dispersion curves (2). In low fields of about 100 μT, a mechanism for the relaxation dispersion of pure water has been shown (19) to be due to the interaction between ^{1}H and ^{17}O which is modulated by intermolecular proton exchange at ~5 kHz. A contrast method directly using different time scales of proton exchange in biological samples is an appealing possibility.

ACKNOWLEDGEMENT

The authors thank Song-I Han for helpful discussions. This work was supported by the Director, Office of Science, Office of Basic Energy Sciences, Division of Materials Sciences and Engineering of the U.S. Department of Energy under Contract No. DE-AC03-76SF00098. M. Möβle acknowledges the “Deutsche Forschungsgemeinschaft” for a postdoctoral fellowship.

REFERENCES

[1] Abragam, A. The principles of nuclear magnetism. Oxford: Clarendon; 1961. p 264.

[2] Macovski A, Conolly S. Novel approaches to low cost MRI. Magn Reson Med 1993;30:221-230.

[3] Stepišnik J, Eržen V, Kos M. NMR imaging in the earth's magnetic field. Magn Reson Med 1990;15:386-391.

[4] Seton HC, Hutchison JMS, Bussell DM. A 4.2 K receiver coil and SQUID amplifier used to improve the SNR of low-field magnetic resonance images of the human arm. Meas Sci Technol 1997;8:198-207.

[5] Koenig SH, Brown RD III. Relaxometry of Tissue. In: Gupta RK, editor. NMR Spectroscopy of Cells and Organisms. Vol. II. Boca Raton FL: CRC Press; 1987. p 75-114.

[6] Koenig SH, Brown RD III. Field-cycling relaxometry of protein solutions and tissue: implications for MRI. Progress in NMR Spectroscopy 1990;22:487-567.

[7] Noack F. NMR field-cycling spectroscopy: principles and applications. Progress in NMR Spectroscopy 1986;18:171-276.

[8] Planinšič G, Stepišnik J, Kos M. Relaxation-time measurement and imaging in the earth's magnetic field. J Magn Reson Ser. A 1994;110:170-174.

[9] Carlson JW, Goldhaber DM, Brito A, Kaufman L. MR relaxometry imaging: work in progress. Radiology 1992;184:635-639.

[10] Rommel E, Kimmich R, Körperich H, Kunze C, Gersonde K. $T_{1\rho}$ dispersion imaging and localized $T_{1\rho}$ dispersion relaxometry: application *in vivo* to mouse adenocarcinoma. Magn Reson Med 1992;24:149-157.

[11] McDermott R, Lee S-K, ten Haken B, Trabesinger AH, Pines A, Clarke J. Microtesla MRI with a superconducting quantum interference device. PNAS 2004;101:7857-7861.

[12] McDermott R, Kelso N, Lee S-K, Möβle M, Mück M, Myers W, ten Haken B, Seton HC, Trabesinger AH, Pines A, Clarke J. SQUID-detected magnetic resonance imaging in microtesla magnetic fields. J Low Temp Phys, 2004;135:793-821.

[13] Volegov P, Matlachov AN, Espy MA, George JS, Kraus RH Jr. Simultaneous magnetoencephalography and SQUID detected nuclear magnetic resonance in microtesla magnetic fields. Magn Reson Med, in press.

[14] Seton HC, Bussell DM, Hutchison JMS. Liquified gas cryostat. UK patents GB2331798 and GB2351549.

[15] Clarke J. SQUID Fundamentals. In: Weinstock H, editor. SQUID Sensors: Fundamentals, Fabrication and Applications. Dordrecht, The Netherlands: Kluwer Academic; 1996. p 1-62.

[16] Mansfield P, Morris PG. NMR imaging in biomedicine. London: Academic Press; 1982. p 17.

[17] Bottomley PA, Foster TH, Argersinger RE, Pfeifer LM. A review of normal tissue hydrogen NMR relaxation times and relaxation mechanisms from 1-100 MHz: dependence on tissue type, NMR frequency, temperature, species, excision, and age. Med Phys 1984;11:425-448.

[18] Winter F, Kimmich R. NMR field-cycling relaxation spectroscopy of bovine serum albumin, muscle tissue, micrococcus luteus and yeast: ^{14}N-^{1}H-quadrupole dips. Biochim Biophys Acta 1982;719:292-298.

[19] Graf V, Noack F, Béné GJ. Proton spin T_1 relaxation dispersion in liquid H_2O by slow proton-exchange. J Chem Phys 1980;72:861-863.

Figure captions

Figure 1

Experimental configuration. (a) SQUID-based second-order gradiometer with room temperature electronics. I_b is the SQUID bias current; pc, ic, and sq label the pickup coil, input coil, and SQUID, respectively. (b) MRI coils and the liquid helium cryostat which houses the gradiometer. For clarity, dB_z/dy coils are not shown.

Figure 2

(a) Pulse sequence for T_1-weighted contrast imaging in a variable field with corresponding evolution of longitudinal magnetization. The polarizing field B_p is adiabatically switched from B_{p1} to B_{p2} and the spins relax towards equilibrium magnetization under B_{int}, the quadrature sum of B_{p2} and $B_{0.}$ Both B_{p2} and B_0 can be adjusted to create the desired B_{int} for T_1 measurement. After a time t_{int}, this field is switched adiabatically to the detection field of 132 μT and a standard imaging sequence is applied following a $\pi/2$ pulse. (b) Field-cycling inversion recovery sequence with corresponding evolution of longitudinal magnetization. Magnetization evolutions are shown for two tissues which have similar values of T_1 in B_{p1} and B_{p2} but very different T_1 in B_0.

Figure 3

(a) Relaxation rate dispersion of 0.25% and 0.5% agarose gel in water measured over the frequency range 72 Hz to 12.8 MHz. The arrows on the lower horizontal axis indicate the fields in which the T_1 contrast was obtained in the following images. (b) Images of a phantom consisting of 0.25% and 0.5% agarose in water weighted by T_1 in four different fields. The pulse sequence of Fig. 2a was used with B_{p1} = 300 mT, B_0 = 132 μT (except in the upper left image where B_0 = 56 μT because the available current from our power supply limited the strength of the counter-field.), t_{int} = 400 ms, and maximum gradient G = 50 μT/m. The polarization time t_p was 2 s for the images with three lowest values of B_{int}, and 1.6 s for B_{int} = 300 ms. Intensity plots along the lines connecting the two gel components are also shown for the two lower images.

Figure 4

Inversion recovery images showing T_1-weighted contrast at 132 μT obtained using the pulse sequence of Fig. 2b with $B_{p1} = B_{p2}$ = 300 mT, B_0 = 132 μT, t_{p1} = 2 s, and t_{int} = 200 ms. The phantom consists of three glass tubes filled with water, and with 0.25% and 0.5% concentrations of agarose gel in water. Because of the different levels of magnetization at the end of the low-field evolution period (t_{int} = 200 ms), the signal from one of the columns is suppressed by choosing t_{p2} so that the magnetization of that column crosses zero at the end of the inversion recovery sequence.

Figure 1

a

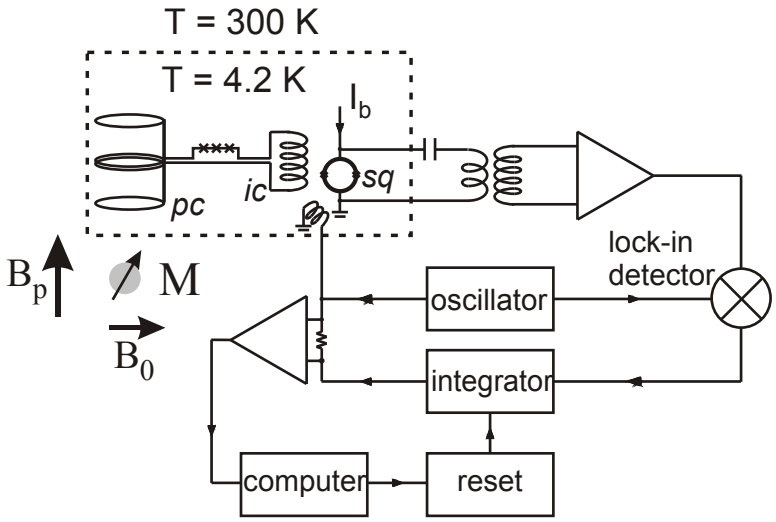
T = 300 K
T = 4.2 K
I_b
pc
ic
sq
B_p
M
B_0
lock-in
detector
oscillator
integrator
computer
reset

b

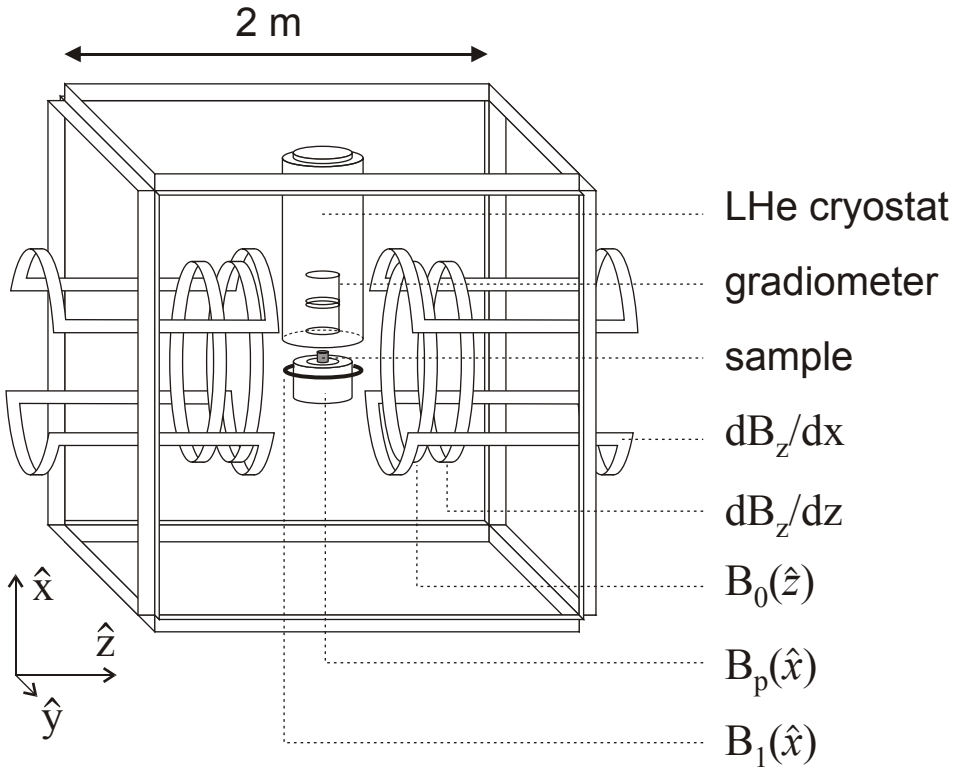
2 m
LHe cryostat
gradiometer
sample
dB_z/dx
dB_z/dz
$B_0(\hat{z})$
$B_p(\hat{x})$
$B_1(\hat{x})$
$\hat{x}$
$\hat{z}$
$\hat{y}$

Figure 2

a

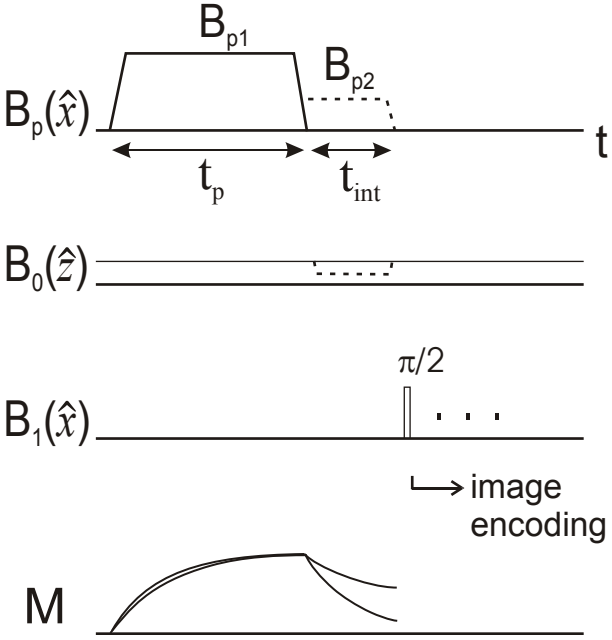
B_{p1}
B_{p2}
$B_p(\hat{x})$
t
t_p
t_{int}
$B_0(\hat{z})$
π/2
$B_1(\hat{x})$
image
encoding
M

b

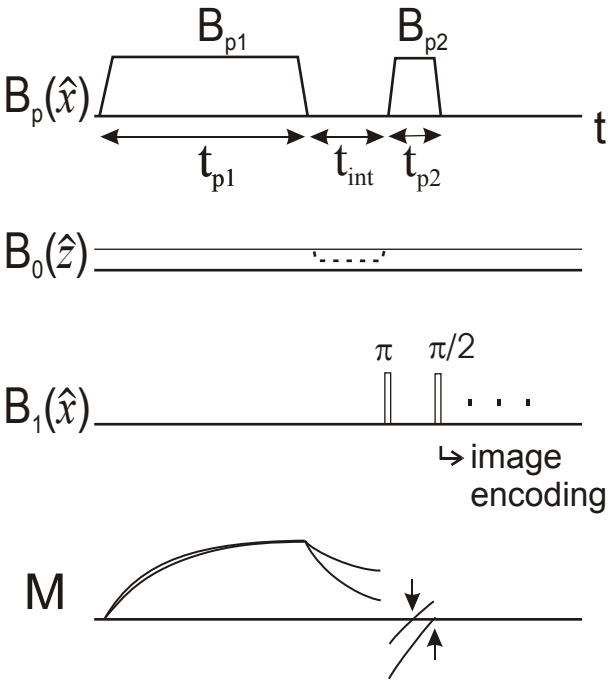
B_{p1}
B_{p2}
$B_p(\hat{x})$
t
t_{p1}
t_{int}
t_{p2}
$B_0(\hat{z})$
π
π/2
$B_1(\hat{x})$
image
encoding
M

Figure 3

a

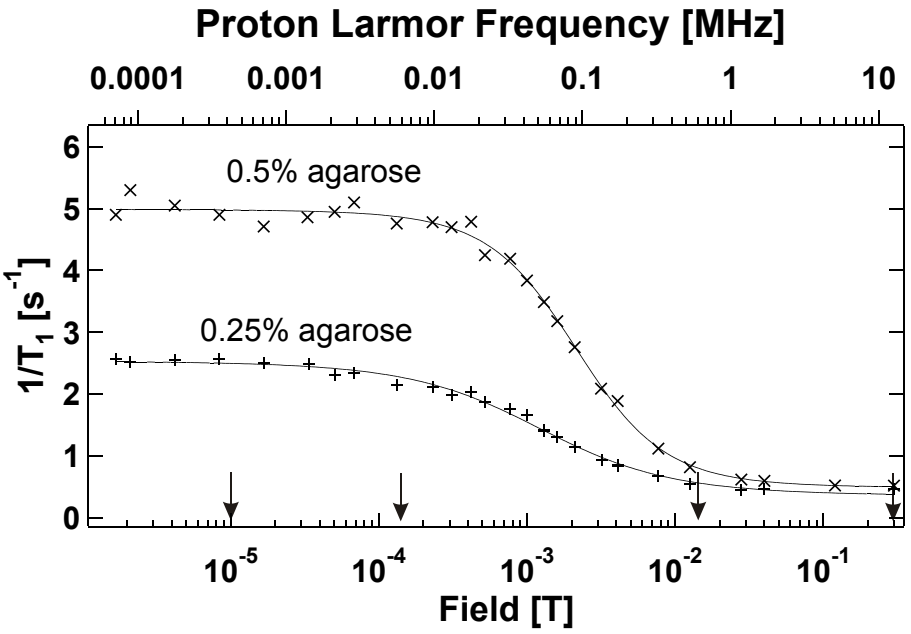
Proton Larmor Frequency [MHz]
0.0001
0.001
0.01
0.1
1
10
0.5% agarose
0.25% agarose
1/T1 [s-1]
Field [T]

b

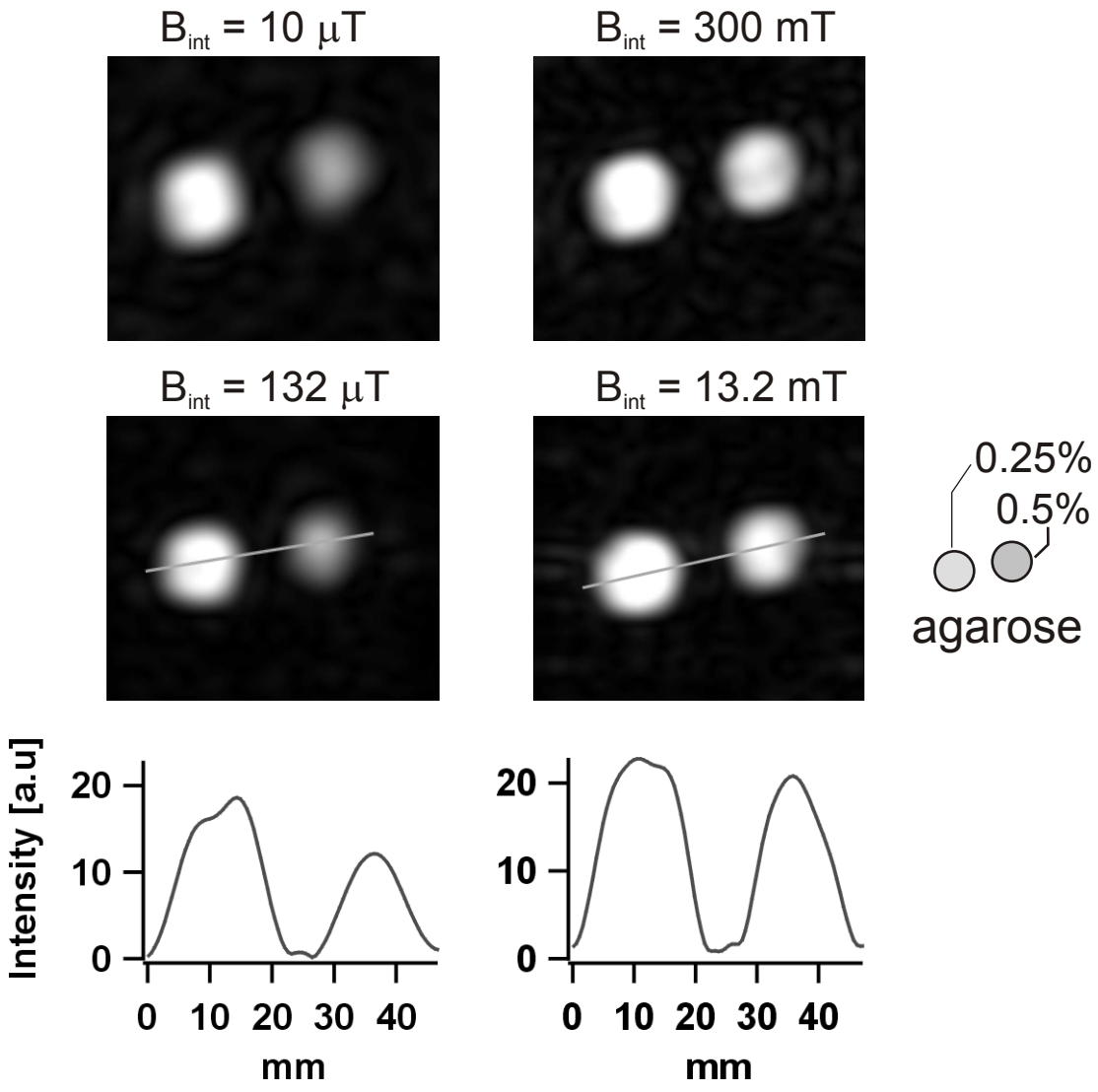
Bint = 10 μT
Bint = 300 mT
Bint = 132 μT
Bint = 13.2 mT
0.25%
0.5%
agarose
Intensity [a.u]
mm
mm

Figure 4

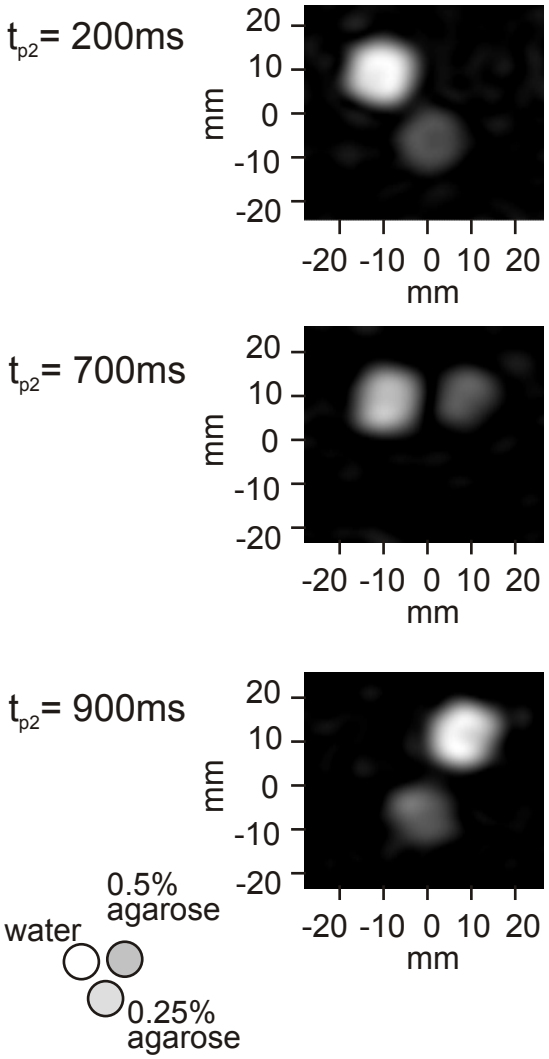
t_{p2}= 200ms
t_{p2}= 700ms
t_{p2}= 900ms
20
10
0
-10
-20
mm
-20 -10 0 10 20
mm
water
0.5% agarose
0.25% agarose